Progress In Electromagnetics Research Letters, Vol. 11, 93–102, 2009

COMPUTATIONAL MODELING OF INDUCTION HEATING PROCESS

M. H. Tavakoli, H. Karbaschi, and F. Samavat

Physics Department
Bu-Ali Sina University
Hamedan 65174, Iran

Abstract—An accurate 2D steady state mathematical model for induction heating process is described and additional results of electromagnetic field, eddy currents distribution and volumetric heat generation have been computed for a sample setup using a finite element method. For the calculations, the input voltage of induction coil is set to be 200 V with a frequency of 10 kHz. It was shown that for the case considered here, the distribution of eddy currents density along the radius/thickness of the workpiece has a damped sinusoidal wave-shaped form.

1. INTRODUCTION

Radio frequency induction heating is a non-contact heating process and has the greatest application in material processing such as heat treating, joining, welding, brazing, soldering, melting and testing. Induction heating is the process of heating an electrically conducting material (usually a metal) by electromagnetic induction, where eddy currents are generated within the workpiece and resistance leads to Joulean heating (I^2R) of the material in the form of temporal and spatial volumetric heating. Induction heating provides a number of advantages such as: quick heating, high production rates, ease of automation and control, and safe and clean working [1–3].

An induction heating installation has three important parts: a source of high-frequency alternating current, an induction coil (RF-coil) and the workpiece (metallic material) to be heated. The RF-coil establishes an alternating electromagnetic field in the setup which induces tremendous currents to flow through the workpiece. These are known as eddy currents. In this aspect, the amount of induced

Corresponding author: M. H. Tavakoli (mht@basu.ac.ir).

eddy currents and power as well as their spatial distribution in the workpiece are the major parameters to be determined. Understanding the physics of these properties is quite crucial and important when designing induction heating systems.

In this article, at first we explain a two dimensional steady state mathematical model for induction heating process and then detailed specifications of electromagnetic field distribution, eddy currents pattern and heating structure in a system are described.

2. MATHEMATICAL MODEL

For calculating an electromagnetic field it is necessary to solve Maxwell's equations [1–3]. In order to solve these equations for our purpose, we have to make several assumptions: (1) The system is rotationally symmetric about the z-axis, i.e., all quantities are independent of the azimuthal coordinate ϕ, (2) all materials are isotropic, non-magnetic and have no net electric charge, (3) the displacement current is neglected, (4) the distribution of electrical current (also voltage) in the RF-coil is uniform, (5) the self-inductance effect in the RF-coil is taken into account, (6) the currents (impressed and induced) have a steady state quality and as a result the electromagnetic field quantities are harmonically oscillating functions with a fixed single frequency.

Under these assumptions, Maxwell's equations in differential form and in the "mks" units (meter-kilogram-second-coulomb) can be written as:

$$\nabla \cdot \mathbf{E} = 0 \quad \text{(from Gauss's law)} \tag{1}$$

$$\nabla \cdot \mathbf{B} = 0 \quad \text{(from Gauss's law)} \tag{2}$$

$$\nabla \times \mathbf{B} = \mu \mathbf{J} \quad \text{(from Ampere's law)} \tag{3}$$

$$\nabla \times \mathbf{E} = -\frac{\partial \mathbf{B}}{\partial t} \quad \text{(from Faraday's law)} \tag{4}$$

$$\mathbf{J} = \sigma \mathbf{E} \tag{5}$$

where $\mathbf{E}$ is the electric field intensity, $\mathbf{B}$ is the magnetic flux density, $\mathbf{J}$ is the free charge current density, μ is the magnetic permeability and σ is the electrical conductivity of the medium, which is a non-zero value only in metallic parts.

Introducing the vector potential $\mathbf{A}$ as

$$\mathbf{B} = \nabla \times \mathbf{A} \tag{6}$$

and assuming axi-symmetric condition, we can transform Eqs. (1)–(5)

into a simple scalar equation [4, 5]

$$\frac{\partial}{\partial r}\left(\frac{1}{r}\frac{\partial \Psi_B}{\partial r}\right)+\frac{\partial}{\partial z}\left(\frac{1}{r}\frac{\partial \Psi_B}{\partial z}\right)=-\mu J_\phi \tag{7}$$

in which Ψ_B is the *magnetic stream function* defined by $\Psi_B(r,z,t) \equiv rA_\phi(r,z,t)$, where A_ϕ is the azimuthal component of $\mathbf{A}$ and (r,ϕ,z) is the cylindrical coordinates. In other words, we assume that all currents (driving and induced) flows only in the azimuthal direction both in the coil and the workpiece.

If we include the self-inductance effect in the induction coil as eddy currents represented by $J_e = -(\sigma_{co}/r)(\partial\Psi_B/\partial t)$, then

$$J_\phi = \begin{cases} J_d + J_e = J_d - \frac{\sigma_{co}}{r}\frac{\partial \Psi_B}{\partial t} & \text{driving and eddy currents in the coil} \\ J_e = -\frac{\sigma_w}{r}\frac{\partial \Psi_B}{\partial t} & \text{eddy currents in the workpiece} \end{cases} \tag{8}$$

where σ_{co} and σ_w are the electrical conductivity of the RF-coil and workpiece, respectively. Setting $J_d = J_0 \cos\omega t$ as the driving current in the coil we can find a solution of the form

$$\Psi_B(r,z,t) = C(r,z)\cos\omega t + S(r,z)\sin\omega t \tag{9}$$

where $C(r,z)$ is the in-phase component and $S(r,z)$ is the out-of-phase component of the solution.

Now the coupled set of elliptic PDE's for $C(r,z)$ and $S(r,z)$ is:

$$\frac{\partial}{\partial r}\left(\frac{1}{r}\frac{\partial C}{\partial r}\right)+\frac{\partial}{\partial z}\left(\frac{1}{r}\frac{\partial C}{\partial z}\right)=\begin{cases} -\mu_{co}\left(J_0-\frac{\sigma_{co}\omega}{r}S\right) & \text{coil} \\ \frac{\mu_w\sigma_w\omega}{r}S & \text{workpiece} \\ 0 & \text{elsewhere} \end{cases} \tag{10}$$

$$\frac{\partial}{\partial r}\left(\frac{1}{r}\frac{\partial S}{\partial r}\right)+\frac{\partial}{\partial z}\left(\frac{1}{r}\frac{\partial S}{\partial z}\right)=\begin{cases} -\mu_{co}\frac{\sigma_{co}\omega}{r}C & \text{coil} \\ -\frac{\mu_w\sigma_w\omega}{r}C & \text{workpiece} \\ 0 & \text{elsewhere} \end{cases} \tag{11}$$

After solving (10) and (11) for $C(r,z)$ and $S(r,z)$, the eddy currents distribution and the energy dissipation rate can be computed via

$$\begin{aligned} J_e &= \frac{\sigma_w\omega}{r}[C(r,z)\sin\omega t - S(r,z)\cos\omega t] \\ &= J_S\sin\omega t + J_C\cos\omega t \end{aligned} \tag{12}$$

and

$$P(r,z,t)=\frac{J_\phi^2}{\sigma}$$
$$=\begin{cases} \frac{\sigma_{co}\omega^2}{r^2}\left[C^2\sin^2\omega t+\left(\frac{J_0 r}{\sigma_{co}\omega}-S\right)^2\cos^2\omega t+C\left(\frac{J_0 r}{\sigma_{co}\omega}-S\right)\sin 2\omega t\right] & \text{coil} \\ \frac{\sigma_w\omega^2}{r^2}\left(C^2\sin^2\omega t+S^2\cos^2\omega t-CS\sin 2\omega t\right) & \text{workpiece} \end{cases} \tag{13}$$

Thus, the power is generated in all metallic parts (including RF-coil) as a function of 2ω. The period for this time-dependence is $\tau = 2\pi/\omega = 10^{-4}$ s for a 10 kHz induction system. Since the time-harmonic function is so short, representation of the heat generation by the time averaged quantity is more useful, which we average over one period to obtain the volumetric heat generation rate,

$$q(r,z) = \frac{\omega}{2\pi}\int_0^{2\pi/\omega} P(r,z,t)\ \mathrm{d}t = \begin{cases} \frac{\sigma_{co}\omega^2}{2r^2}\left[C^2 + \left(\frac{J_0 r}{\sigma_{co}\omega} - S\right)^2\right] & \text{coil} \\ \frac{\sigma_w\omega^2}{2r^2}\left(C^2+S^2\right) & \text{workpiece} \end{cases} \tag{14}$$

The boundary conditions are $\Psi_B = 0$; both in the far field $(r, z \to \infty)$ and at the axis of symmetry $(r = 0)$.

2.1. The Calculation Conditions

Values of electrical conductivity employed for our calculations are presented in Table 1 and operating parameters are listed in Table 2. The system under consideration includes a right cylindrical conductor

Table 1. Values of electrical conductivity (mho/cm) used in our calculations; the subscripts *co* and *w* denote coil (*copper*) and workpiece (*steel*), respectively.

Symbol	Value
σ_{co}	5.9×10^5
σ_w	4.0×10^4

Table 2. Operating parameters used for calculations.

Description (units)	Symbol	Value
Workpiece radius (mm)	r_w	55
Workpiece height (mm)	h_w	93
Coil inner radius (mm)	r_{co}	85
Coil width (mm)	L_{co}	10
Coil wall thickness (mm)	l_{co}	1
Height of coil turns (mm)	h_{co}	13
Distance between coil turns (mm)	d_{co}	3

load (i.e., steel workpiece) in the direction of Oz (i.e., Oz is the centerline) which is surrounded by a multiturn cylindrical induction coil with 6 hollow rectangular-shaped copper turns, Figure 1. In a real induction system this coil is usually cooled very efficiently by water flowing inside the coil turns. Therefore it is realistic to assume that the coil is always at room temperature. We assume a total voltage of the coil $V_{coil} = 200\,\mathrm{V}$ with a frequency of 10 kHz. The driving current density in the induction coil is calculated by $J_0 = \sigma_{co} V_{coil}/(2\pi R_{co} N)$, where R_{co} is the mean value of the coil radius and N is the number of coil turns. For the magnetic permeability (μ) we assume that it is everywhere the constant value of free space $\mu = \mu_r \mu_0 \simeq \mu_0$ (i.e., $\mu_r \simeq 1$) where μ_r is the relative magnetic permeability.

The quantity $\delta_w = (2/\mu_w \sigma_w \omega)^{1/2}$ has the dimension of a length and is called the *skin depth* (or penetration depth). It is a measure of the field penetration depth into the conductors. In our calculation the corresponding skin depth of the steel workpiece is $\delta_w = 2.5\,\mathrm{mm}$.

It should be mentioned here that since induction heating is a very complicated process, we can not expect accurate simulation of the whole chain of coupled phenomena — electromagnetic, thermal, mechanical, hydrodynamic and metallurgical — during a heating process. The most important and controllable process is electromagnetic which is analyzed here.

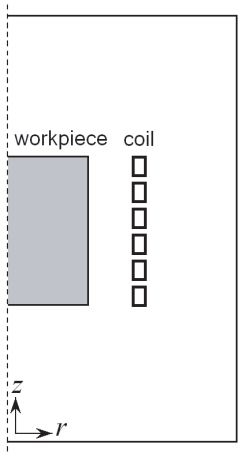

Figure 1. Sketch of the induction heating setup including a right cylindrical workpiece and a multiturn RF-coil.

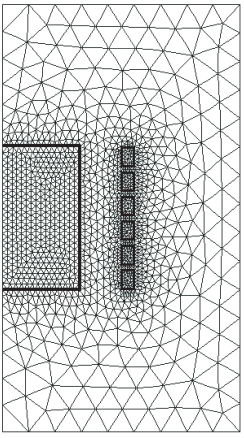

Figure 2. The finite element mesh of the calculation domain. Special fine grid is placed in the areas where resolution of the solutions is expected to be difficult.

2.2. Numerical Method

The involved partial differential equations require using a numerical discretization method to solve them. The calculation of the fundamental equations with boundary conditions have been made by 2D finite element method, Figure 2. After solving the set of equations we can obtain the electromagnetic field and eddy currents distribution as well as the power densities in all parts of the studied system.

The results based on this set of parameters will be presented now.

3. RESULTS AND DISCUSSION

Figure 3 shows the distribution of in-phase component (right hand side) and out-of-phase component (left hand side) of the magnetic stream function. The maximum of in-phase component (C) is located at the lowest and top edges of the RF-coil ($C_{\max} = 3.3 \times 10^{-6}$ weber) while the minimum ($C_{\min} = -3.3 \times 10^{-6}$ weber) is located on the upper and lower corners of the workpiece. For the out-of-phase component (S), the maximum is located at the outer surfaces of the induction coil turns ($S_{\max} = 9.0 \times 10^{-5}$ weber) and its distribution has a linear gradient in the space between the coil and the workpiece. The workpiece tends to force the electromagnetic field components out of its body and makes

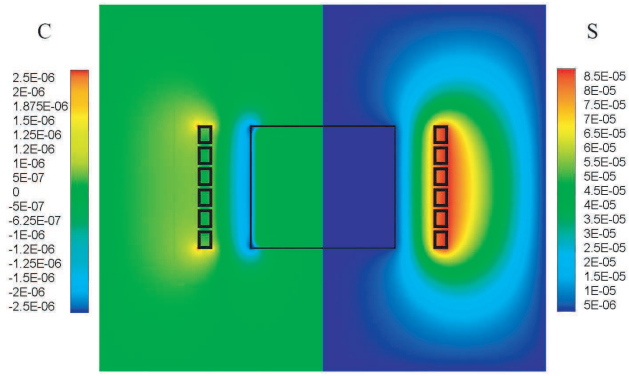

Figure 3. Components of the magnetic stream function (Ψ_B) calculated for the case considered here. The right hand side shows the in-phase component (C) with $C_{\max} = 3.3 \times 10^{-6}$ weber on the lowest and top edges of the RF-coil and $C_{\min} = -3.3 \times 10^{-6}$ weber on the edges of the workpiece. The left hand side shows the out-of-phase component (S) with $S_{\max} = 9.0 \times 10^{-5}$ weber on the outer surfaces of the induction coil turns.

them more intense at the space between the workpiece and the coil compared to other places.

Deformation and distortion of the C-component in the area close to the top and bottom edges of the workpiece and RF-coil is also particularly evident in Figure 3 (edge effect). It is worth to mention that the distribution of the in-phase component (C) depends on the geometry of both induction coil and workpiece, while the out-of-phase component (S) mainly depends on the configuration of RF-coil where the driving current is produced.

Figure 4 shows the radial profile of both components in the middle of the workpiece. It is clear that both components have a damped oscillating behavior. Consequently, the induced electromagnetic field within the workpiece, concentrated near the surface and decay with distance from the surface. It is interesting to note that both components are quite small and also $|S/C| \sim 1$ in the workpiece where the required heat generation occurs. As a result, both components take part to the required heat generation equally, according to Eq. (14).

Figure 5 shows the distribution of in-phase component and out-of-phase component of the eddy currents (i.e., J_C and J_S) in the workpiece. It is seen that the distribution of both components have a damped sinusoidal wave shape which is a result of propagation of the electromagnetic wave in the conductor workpiece [6], Figure 6. In other words, the damped sinusoidal eddy currents flow is produced by damped oscillatory electromagnetic field in the conductor workpiece. Both components are always in the opposite direction to the driving

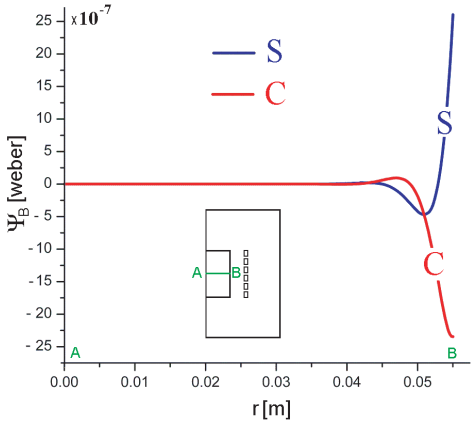

Figure 4. The radial profile of the C and S components along A-B line of the workpiece thickness.

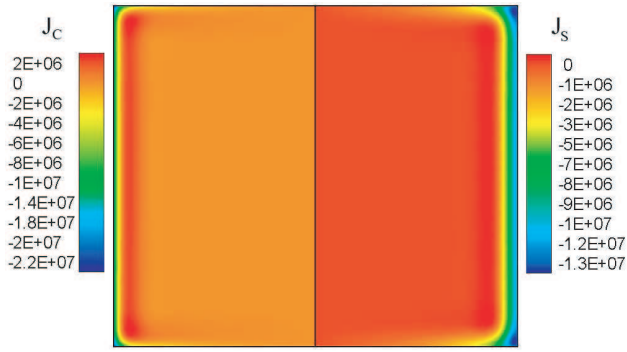

Figure 5. Components of the eddy currents distribution in the workpiece. The right hand side shows the in-phase component (J_C) with $J_C^{\min} = -2.3 \times 10^7\,\mathrm{A/m^2}$ and $J_C^{\max} = 0.4 \times 10^{-7}\,\mathrm{A/m^2}$ and the left hand side shows the out-of-phase component (J_S) with $J_S^{\min} = -1.45 \times 10^7\,\mathrm{A/m^2}$ and $J_S^{\max} = 0.1 \times 10^{-7}\,\mathrm{A/m^2}$. $J_C^{\min}$ and $J_S^{\min}$ are located on both edges while $J_C^{\max}$ and $J_S^{\max}$ are positioned on the area close to both corners.

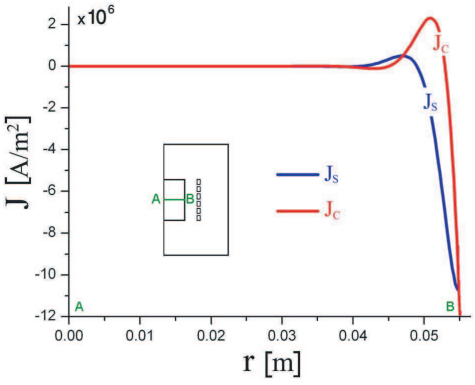

Figure 6. The damped wave-shaped profiles of the eddy currents components along A-B line of the workpiece thickness.

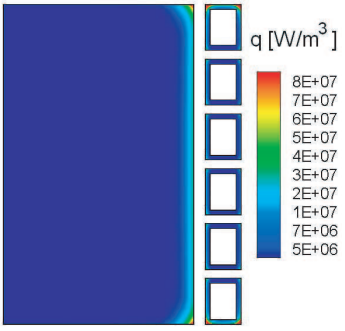

Figure 7. Volumetric power distribution (q) in the workpiece and the RF-coil with $q_{\max}^{workpiece} = 8.5 \times 10^7\,\mathrm{W/m^3}$) on the both corners.

current J_0 (because $J_C < 0$ and $J_S < 0$) on the outer surface of the workpiece side wall. Both $J_C^{\min}$ and $J_S^{\min}$ are located on the both edges of the workpiece and the position of $J_S^{\max}$ as well as $J_C^{\max}$ is in the

workpiece body and close to the ends because of intense edge effect. $J_S^{\min}$ shows the related wave crest which is not true for $J_C^{\min}$. All effective eddy currents are located in a distance of $\approx 6\delta_w$ from the side wall and as a result no current in the inner portion.

The volumetric heat generation rate (q) in the system has been shown in Figure 7. The power intensity is at its maximum value at the both edges of the workpiece (where the $J_C^{\min}$ and $J_S^{\min}$ are located) and falls off about exponentially inward. These are "hot spots" (highly heated areas) which are a direct result of the edge effect and distortion of electromagnetic filed in those areas, Figure 8. The outer surface to core heating difference is a result of the skin effect (the phenomena of nonuniform induced alternative current distribution within the conductor cross section) [1–3]. The appearance of varies heating patterns is caused directly by difference in the eddy currents distribution in the workpiece.

The spatial distribution of heat generation in the induction coil is mostly uniform with local hot spots at the lowest and upper edges. The skin effect and proximity effect (the effect on current distribution in a conductor when another conductor is placed nearby) are responsible for these hot spots. Since the currents (driving and induced) have the

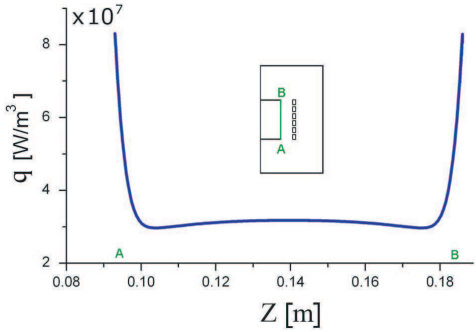

Figure 8. The W-shaped profiles of the heat generated along the outer surface of the workpiece side wall.

Table 3. Detail information about the heat generated in the heating setup.

Part	Heat generated (Watt)	Percentage (%)
workpiece	1481	57
RF-coil	1113	43
Total	2594	100

same direction in the coil turns, the eddy currents will be concentrated on opposite side of the induction coil (i.e., the top and lowest surfaces).

Detail information about the heat generated in the system has been shown in Table 3.

4. CONCLUSION

Detailed specifications of an accurate 2D steady state mathematical model for induction heating process is built to study the electromagnetic field distribution, eddy currents density and heating pattern in the workpiece. From the obtained results we can conclude:

- The finite element (FE) modeling of the induction heating is still a challenging task.
- The spatial structure of electromagnetic field is a complex function of the workpiece and the RF-coil geometry.
- For the case considered here, the currents density distribution along the radius/thickness has a damped sinusoidal wave-shaped form, which is significantly different than the classical exponential distribution.
- Because the current densities are concentrated in the external areas of the workpiece and specially in both edges, the resulting heating density is mainly produced in those areas (external heating) and the internal heating (core heating) will be considerably weak for the operating frequency considered here.

REFERENCES

1. Leatherman, A. F. and D. E. Stutz, *Induction Heating Advances*, National Aeronautics and Space Administration, 1969.
2. Rudnev, V., D. Loveles, R. Cook, and M. Black, *Handbook of Induction Heating*, New York, NY, 2003.
3. Zinn, S. and S. L. Semiatin, *Elements of Induction Heating*, ASM International, 1988.
4. Gresho, P. M. and J. J. Derby, "A finite element model for induction heating of a metal crucible," *J. Crystal Growth*, Vol. 85, No. 1–2, 40–48, 1987.
5. Tavakoli, M. H., "Modeling of induction heating in oxide Czochralski systems — Advantages and problems," *Cryst. Growth Des.*, Vol. 8, No. 2, 483–488, 2007.
6. Reitz, J. R., F. J. Milford, and R. W. Christy, *Foundations of Electromagnetic Theory*, Addison-Wesley, 1993.